A Cost-Effective Hemin-Based Artificial Enzyme Allows for Practical Applications

Dehui Qiu, Fangni He, Yuan Liu, Zhaoxi Zhou, Yuqin Yang, Zhongwen Long, Qianqian Chen, Desheng Chen, Shijiong Wei, Xuanxiang Mao, et al.

A Cost-Effective Hemin-based Artificial Enzyme Allows for Practical Applications

Dehui Qiu, Fangni He, Yuan Liu, Zhaoxi Zhou, Yuqin Yang, Zhongwen Long, Qianqian Chen, Desheng Chen, Shijiong Wei, Xuanxiang Mao, Xiaobo Zhang, Jean-Louis Mergny, David Monchaud, Huangxian Ju, and Jun Zhou**

D. Qiu, F. He, Y. Liu, Z. Zhou, Y. Yang, Z. Long, Q. Chen, D. Chen, S. Wei, X. Mao, X. Zhang, JL. Mergny, H. Ju, J. Zhou, State Key Laboratory of Analytical Chemistry for Life Science, School of Chemistry and Chemical Engineering, Nanjing University, Nanjing 210023, China. E-mail: xhzxb@nju.edu.cn; jun.zhou@nju.edu.cn. J.L. Mergny, Laboratoire d'Optique et Biosciences (LOB), Ecole Polytechnique, CNRS, INSERM, Institut Polytechnique de Paris, 91120 Palaiseau, France. D. Monchaud, Institut de Chimie Moléculaire (ICMUB), CNRS UMR6302, UBFC, 21078 Dijon, France

Abstract

Nanomaterials excel in mimicking the structure and function of natural enzymes while being far more interesting in terms of structural stability, functional versatility, recyclability and large-scale preparation. Herein, we assembled hemin, histidine analogues and G-quadruplex DNA in a catalytically competent supramolecular assembly referred to as assembly-activated hemin enzyme (AA-heminzyme). The catalytic properties of AA-heminzyme were investigated both in silico (by molecular docking and quantum chemical calculations) and in vitro (notably through a systematic comparison with its natural counterpart horseradish peroxidase, HRP). We found that this artificial system was not only as efficient as HRP to oxidize various substrates (with a turnover number k_{cat} of 115 s^{-1}) but also more practically convenient (displaying better thermal stability, recoverability and editability) and more economically viable, with a catalytic cost amounting to less than 10% of that of HRP. The strategic interest of AA-heminzyme was further demonstrated for both industrial wastewater remediation and biomarker detection (notably glutathione, for which the cost was decreased by 98% as compared to commercial kits).

Keywords: Artificial enzyme; hemin; histidine analogue; G-quadruplex

1. Introduction

Artificial enzymes, especially peroxidase mimics, have been widely used in biosensing, cancer therapy, environmental protection and food safety.[1] For replacing natural enzymes, artificial enzymes should meet key requirements: they must reach the level of catalytic activities of corresponding native enzymes while being more practically convenient (usable at high

temperatures, high/low pH, etc.), and must also be less expensive than their native counterparts. Hemin, an inexpensive iron porphyrin derivative, has been extensively used to construct peroxidase-mimicking artificial catalytic systems,[2] a quite active field of research because of the numerous applications of peroxidases for biosensing purposes. Hemin is particularly used in combination with G-quadruplex DNA (or G4 DNA), a thermodynamically stable higher-order DNA structure:[3] the resulting G4/hemin systems, known as G4/hemin DNAzymes or G4-DNAzymes,[4] are currently being exploited in biocatalysis owing to their exquisite properties in terms of versatility, designability and addressability.[5] When included in nanomaterials, hemin-based systems rely on the combination of hemin with carbon nanotubes, graphene, hydrogels, polymers, proteins[6] and peptides[7] to address some of the hemin classical issues, that is, its self-aggregation deactivation and low solubility in aqueous solutions. However, the catalytic activities of these nanomaterials still lag far behind natural enzymes notably the reference enzyme horseradish peroxidase (HRP), which represents a severe limitation to their wider use, a limitation that must be urgently overcome.

The unique properties of HRP originate from its interaction with a heme cofactor, driven by the presence of a well-defined network of amino acid residues in its catalytic center,[10] which highlights the importance of the heme microenvironment. However, HRP suffers from several known limitations, notably related to its biosourced origin which requires an expensive production that furthermore leads to mixtures of HRP isoforms responsible for batch-to-batch variations[8] and poorly reproducible results.[9] Nanomaterial-based mimetic enzymes are a reliable alternative to the use of HRP, as their synthesis and characterizations are controlled, which ensures a better reproducibility. In this context, we recently reported on a very active system named chimeric peptide DNAzyme, or CPDzyme, in which we recapitulated such a peptide/DNA microenvironment to provide an artificial enzyme displaying a higher turnover number (k_{cat}) than HRP,[2b] in addition to be more chemically robust. The only sour note was its preparation, found to be complex and expensive, which represents a serious obstacle to large-scale applications. To tackle this issue, we wondered whether we could construct an efficient and cost-effective peroxidase-mimicking system *via* a simple, one-pot assembly of hemin, peptide, DNA and/or other molecules in a CPDzyme manner but without the burden of covalent assembly.

We thus proposed here the new concept of assembly-activated hemin enzyme, or AA-heminzyme. On the basis of the significant role of histidine (His) in both HRP and CPDzyme catalytic center, which acts as both a proximal iron ligand and a distal acid-base catalyst (**Figure 1**A), we first assembled Fmoc-Histidine (F), hemin (h) and His analogues (such as imidazole

(I) for example) in a complex referred to as Fmoc-Histidine/hemin/imidazole (FhI). Then, a G4 structure was added to provide a Fmoc-Histidine/G4/hemin/imidazole (FG4hI) complex, which forms the very heart of AA-heminzymes. As further demonstrated below, this system exhibits several advantages when compared to HRP, including high catalytic performance, chemical robustness and recyclability, along with a lower cost. Also, AA-heminzymes could be easily modified to achieve new functions: for instance, we show here that FG4hI could be coupled with luminol (L) to result in FG4hIL system (**Figure 1**B) to detect glutathione (GSH) with the same efficiency and sensitivity than commercial kits with a far lower cost (only 2%), highlighting the huge potential of our AA-heminzyme system.

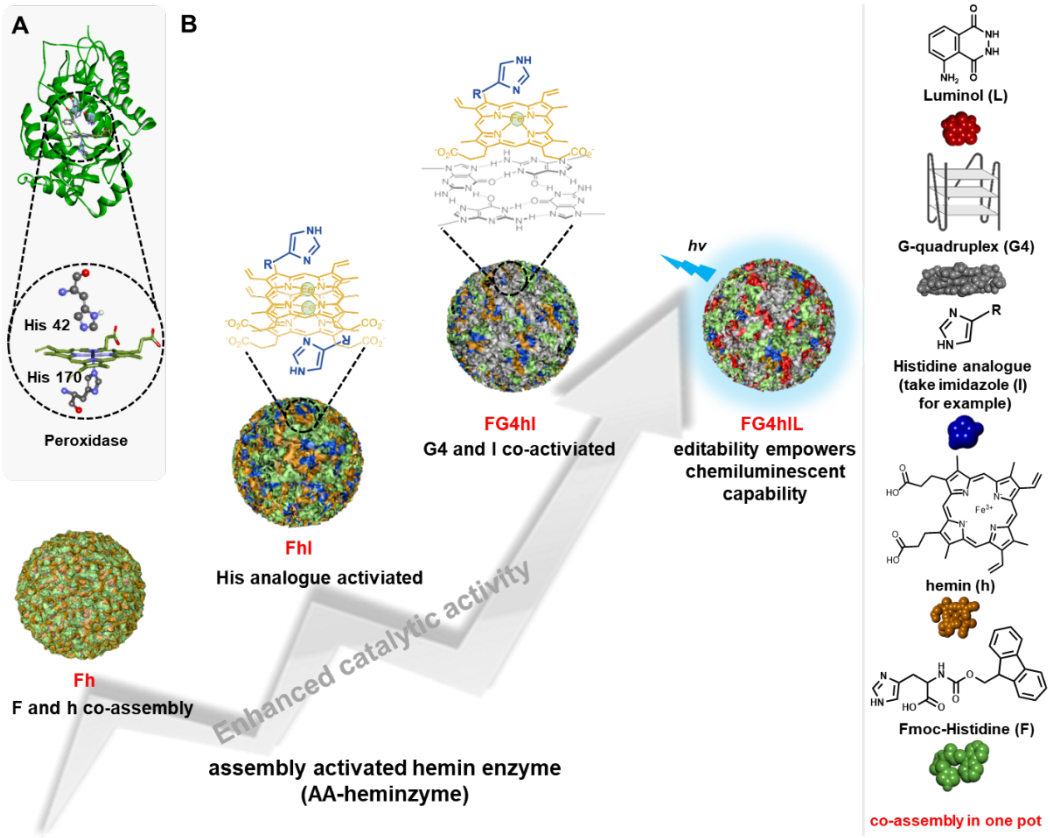

Figure 1. (A) Key amino acid residues in the heme-binding region of HRP. (B) Schematic representation of the assembly of hemin with His analogues: for instance, if imidazole (I) is used, the corresponding complex is FhI, upon addition of G4 it becomes FG4hI, and upon addition of luminol it becomes FG4hIL. All these complexes are used as AA-heminzymes for catalyzing peroxidase-like reactions.

2. Results and Discussion

2.1. Synthesis and characterization of AA-heminzyme

AA-heminzyme was obtained simply by mixing His analogues (to serve as proximal/distal amino acid), hemin (cofactor), G4s (to activate hemin) and luminol (if needed) *via* hydrophobic effect and π-π stacking interaction of the Fmoc group (**Figure 1**B),[11] and the preparation details are shown in supporting information. All AA-heminzymes were solid spherical

nanoparticles, as demonstrated by transmission electron microscopy (TEM) (**Figure S1**). Dynamic light scattering (DLS) showed that the hydrodynamic diameters of Fh, FhI, FG4hI and FG4hIL were 284 ± 14, 299 ± 8, 315 ± 22 and 327 ± 18 nm, respectively (**Figure S2**A-D). The zeta potential was determined to assess the charges of AA-heminzyme and the values found (between -15 to -40 mV, **Figure S2**E) demonstrate the stability of the nanoparticles. UV-Vis absorption spectroscopy showed that hemin was incorporated as both a monomer and a dimer hemin,[12] that the addition of F (Fh complex) resulted in widening and redshift of the Soret band, indicating the formation of typical disorderly J-aggregates of hemin (**Figure S3**A-C),[13] and that of I (FhI complex) triggers a charge transfer from I to hemin, confirming their coordination (**Figure S3**D).[14] The participation of different His analogues and G4 in AA-heminzyme, and the successful synthesis of FG4hIL were confirmed by UV-Vis spectra (**Figures S4** and **S5**). Finally, the actual concentration of iron within the different complexes (Fh, FhI and FG4hI) was quantified by ICP-MS and found to be between 4.8 ± 0.1 and 6.2 ± 0.1 μM (**Figure S6**).

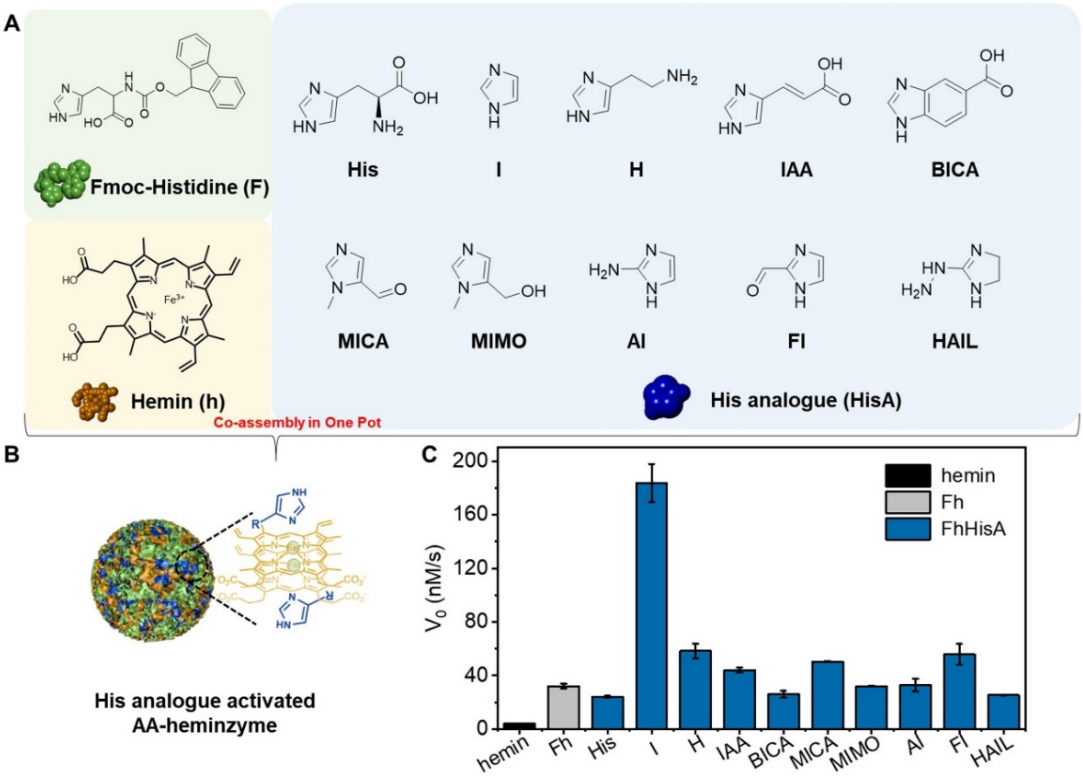

Figure 2. (A,B) Chemical composition of Fmoc-Histidine/hemin/histidine analogues (FhHisA) mimetic enzymes. (C) The catalytic activity (H_2O_2-promoted ABTS oxidation) of hemin, Fh and FhHisA mimetic enzymes.

2.2. Screening for the best activators

The activating role of His analogues within AA-heminzymes[15] was investigated in a systematic manner: nine His analogues (shown in **Figure 2**A) were assembled within AA-

heminzymes (**Figure 2**B) and their catalytic activity evaluated by the model oxidation reaction of 2,2'-azino-bis (3-ethylbenzothiazoline-6-sulfonic acid) (ABTS) in the presence of H_2O_2.

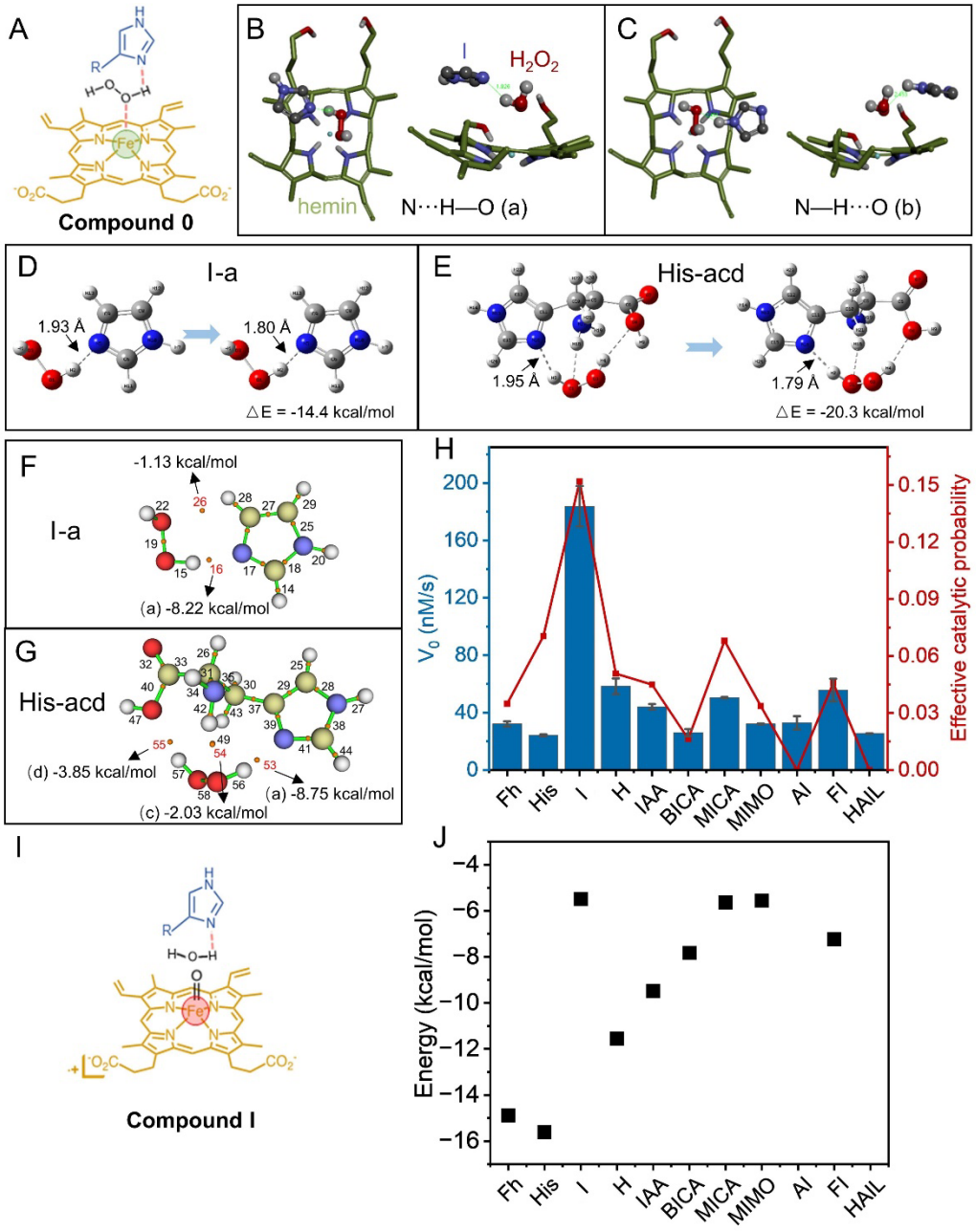

Figure 3. (A) Schematic representation of His analogue assisted H_2O_2 binding to hemin in compound 0. (B and C) Docking results of the H-bond formation between I and H_2O_2 of either (B) a- or (C) b-type. (D and E) Calculations of the energy of interaction between (D) I, (E) His and H_2O_2. (F and G) Hydrogen bonding energy between (F) I-a, (G) His-acd and H_2O_2. (H) Comparison of calculated (red line) *versus* experimental catalytic activities (blue bar). (I) Schematic representation of compound I of His analogue releasing water. (J) Energy involved in breaking all the hydrogen bonds between His analogues and water during the dehydration step.

As seen in **Figure 2**C, the catalytic rate of Fh alone was 32.1 nM· s^{-1}, which was 7.8-fold higher than that of free hemin. Interestingly, the addition of I, histamine (H), (2E)-3-(1H-

Imidazole-4-yl) acrylic acid (IAA), 1-Methyl-5-imidazole carboxaldehyde (MICA) and 2-Formylimidazole (FI) to Fh further increased this activity, the best enhancement being obtained with I, which led to a catalytic rate of 183.7 nM· s^{-1}, found to 44- and 5.7-fold higher than that of hemin and Fh, respectively. It should be noted that catalytic activity of the AA-heminzyme were affected by the ratio among different blocks: for example, when the concentration of hemin was fixed at 1 mM, the highest catalytic rate, which was 232.0 nM· s^{-1}, was achieved at molar ratios of 6 and 5 for F and I, respectively (**Figure S7**).

2.3. Theoretical calculation of the activation mechanism

To further understand the activation role of His analogues in the catalytic systems described above, molecular docking and quantum chemical calculations were implemented. We first focused on the formation of compound 0 (**Figure 3**A). To this end, the ability of the nitrogen atom in His analogues to act as an acid-base catalyst when binding H_2O_2 in compound 0 was calculated: as seen in **Table S1**, a large number of predicted conformations were generated by docking (AutoDock Vina)[16] with a relatively high level of spatial accuracy; all intermolecular hydrogen (H-)bonds were classified according to whether they might facilitate the catalytic bonding process or not, following an intermolecular force analysis of all possible output conformations. For instance, N···H—O (a-type) and N—H···O (b-type) H-bonds in I were artificially defined as promoting and inhibiting H-bonds, respectively (**Figure 3**B,C). Notably, some molecules may generate complex situations, as shown in **Figure S8**, where His and H_2O_2 formed four states respectively His-a, His-ac, His-ad and His-acd, which contain a-type hydrogen bonds as well as inhibiting NH_2···O (c- type) and COOH···H/O (d-type) hydrogen bonds. We statistically analyzed the conformation of 11 molecules containing promoting (a-type) H-bonds (**Table S1**) and selected the most stable conformations for further structural optimization and energy calculations with high accuracy (Gaussian software, **Figure 3**D,E). The energy (ΔE) of the interaction between these conformations and H_2O_2 were calculated (**Table S2**), the H-bonding energy predicted (Multiwfn)[17] and then ranked (**Figure 3**F,G and **Table S3**). The conformational frequency of effective H-bonds (in molecular docking) and effective H-bond energy ratio in each conformation (in Gaussian) were multiplied to obtain the effective catalytic probability (**Figure 3**H and **Table S4**) which was found to be roughly consistent with the experimental results (V_0, **Figure 2**C).

We then investigated the fate of compound I (**Figure 3**I). To this end, the ability of active N in compound I to release the produced H_2O molecule was simulated: the H_2O_2 used in the previous model was replaced by H_2O and this new model was structurally optimized (Gaussian)

and the parameters used above regarding H-bond were calculated. In addition, the binding energy required for the release of H_2O from His analogues was also determined (**Table S5**). The energy required to break all H-bonds during the dehydration process was summarized in **Figure 3**J. For some His analogues, this process requires the breaking of not only a-type but also other types of H-bonds, which greatly reduced the dehydration capacity. In contrast, I, MICA and MIMO exhibited excellent dehydration ability as no new H-bond was formed during the dehydration step. The difference in the overall catalytic performance between I and both MICA and MIMO (Figure 3H, blue bars) thus originates in the difference in H_2O_2 binding (Figure 3H, red curve) as their H_2O releasing capacity are the comparable (Figure 3J). Altogether, these *in silico* investigations allowed for extracting a series of criteria for evaluating the catalytic ability of H_2O_2/hemin-based peroxidase-mimicking enzymes and provided unique insights into how natural HRP avoids the formation of inhibitory H-bonds, the donating groups in its catalytic center being involved in H-bond with neighboring amino acids.[10a]

2.4. G-quadruplex DNA further enhances the catalytic activity

The results of the calculations described above indicate that I is an excellent catalytic activator, acting at both substrate binding and product releasing steps (**Figure 3**H,J). However, hemin dimerization, which is one of the most critical limitations of hemin-based peroxidase-mimicking enzymes, cannot be hampered by I. To tackle this issue, a G4 unit was used in light of its known ability to strongly interact with hemin by π-π stacking,[3,18] which consequently preclude its dimerization. FG4hI was thus prepared (**Figure 1**B) and the G4 fold of all the sequences used (**Table S6**) was confirmed by circular dichroism (CD, **Figure S9**). FG4hI displayed an enhanced catalytic activity (**Figure 4**A), as demonstrated by the 2.9-fold increment (from 225 to 655 $nM\cdot s^{-1}$) when parallel G4s were added, which even reaches 1551 $nM\cdot s^{-1}$ when using G4s with flanking dCT and dTC at both 5' and 3' ends,[19] being thus 6.9- and 41.3-fold more active than FhI and Fh, respectively. This activation effect disappeared when the sequence used was unable to fold into a G4 structure (mut-G4). We thus report here on an unprecedented co-activation phenomenon promoted by the concomitant action of I and G4 (**Figure 4**B): we propose that hemin interacts first with G4 *via* π-π stacking interaction; then, the distal base C of the G4 forms H-bonds with H_2O and helps I capture H_2O_2 to form compound 0, thus promoting the coordination of H_2O_2 to the iron center, facilitating the cleavage of the O-O bond and accelerating the formation of compound I; when encountering a first molecule of ABTS, compound I is reduced to compound II and produces $ABTS^{\cdot+}$; the second ABTS molecule reduces compound II to the native state of the Fe^{III} and produces another molecule of

$ABTS^{\cdot+}$. Since the generation of compound I is the rate-determining step of the whole catalytic reaction,[19b] the co-activation effect of I and G4 is thus critical.

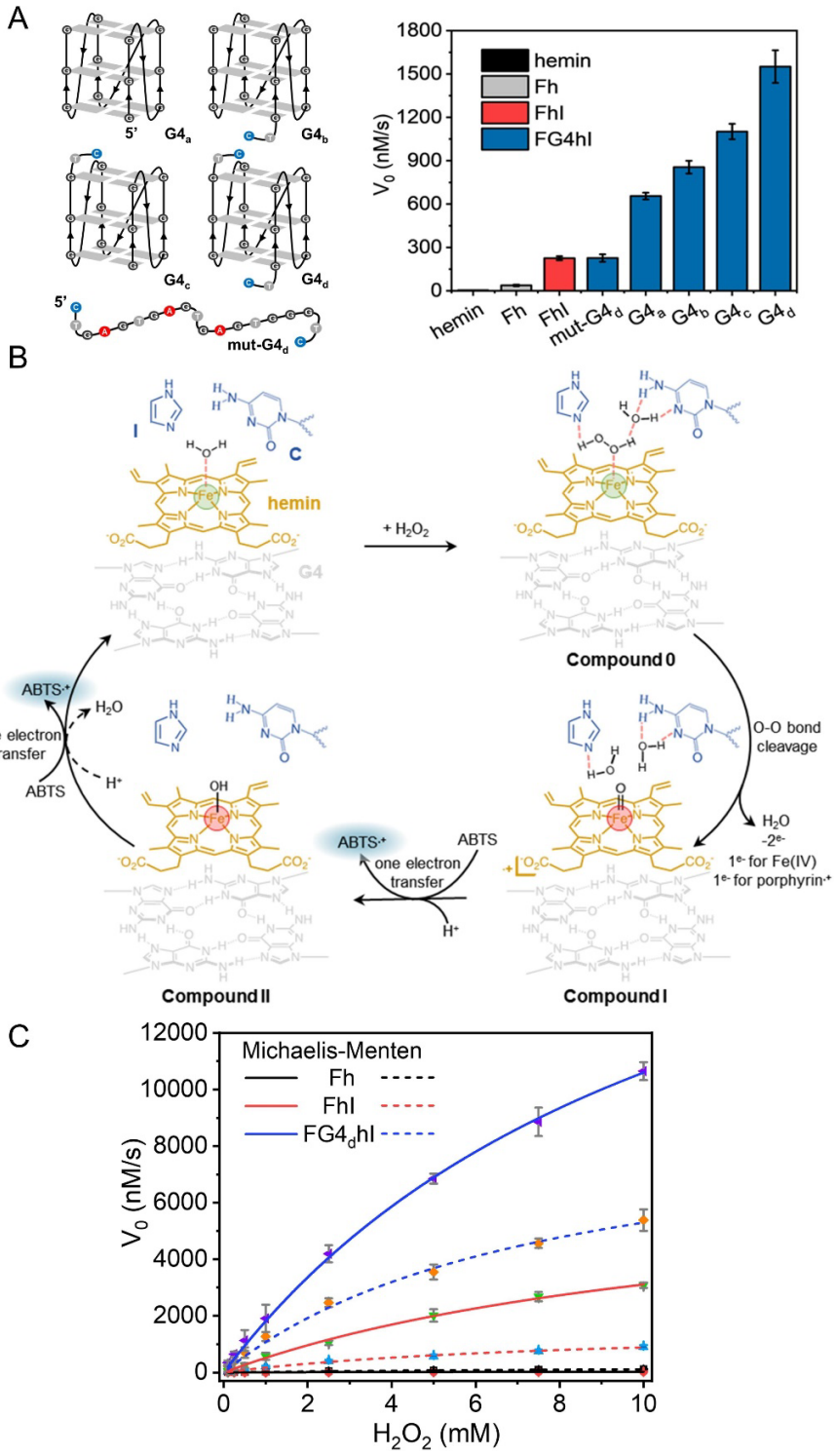

Figure 4. (A) The effect of different G4 sequences on the catalytic activity of the corresponding AA-heminzymes. (B) Proposed catalytic cycle of FG4hI-assisted oxidation of ABTS by H_2O_2. Green and red spheres represent Fe(III) and Fe(IV), respectively. (C) Saturation curves of the oxidation of ABTS catalyzed by Fh, FhI and $FG4_dhI$ at different concentrations of H_2O_2. The solid and dashed lines represent the Michaelis-Menten fitting curves at pH 5 and 7, respectively. Experiments were performed in 10 mM Britton-Robinson buffer (pH 5 and 7, 100 mM K^+) containing 200 nM AA-heminzyme and 5 mM ABTS.

2.5. Performance and cost of AA-heminzyme

To better characterize these catalytic oxidation reactions, the steady-state kinetic curves of Fh, FhI and FG4$_d$hI were analyzed. First, the optimal pH changed from pH 7 for Fh to pH 5 for FhI and FG4$_d$hI (**Figure S10**); the kinetic parameters were thus determined at these two pH values. As shown in **Figure 4**C and **Table 1**, the turnover number (k_{cat}) values at pH 5 and 7 were 0.326 and 1.09 s^{-1} for of Fh, 35.1 and 8.23 s^{-1} for FhI, and 115 and 47.1 s^{-1} for FG4$_d$hI (corresponding to an improvement > 352-fold at pH 5, and > 43-fold at pH 7). FG4$_d$hI thus reached a k_{cat} value which is 383-fold higher than the common G4/Hemin system (k_{cat} = 0.3 s^{-1}),[20] that is, in the same order of magnitude than HRP (k_{cat} = 50-800 s^{-1}).[21] The K_m values also decreased (from 13.8 to 11.6 mM at pH 5; from 9.37 to 7.78 mM at pH 7, **Table 1**). Additionally, the K_m (ABTS) values with another substrate, ABTS, were also decreased (**Figure S11**). These results demonstrate that the activation effect not only boosts the overall catalytic efficiency but also enhances the affinity of the enzyme for its substrates.

Table 1. Steady-state kinetic parameters of Fh, FhI and FG4$_d$hI at pH 5 and 7.

Catalysts	pH	K_m (mM)	v_{max} (μM s^{-1})	k_{cat} (s^{-1})	k_{cat} / K_m (mM^{-1} s^{-1})
Fh	5	13.8	0.0653	0.326	0.0236
	7	9.37	0.218	1.09	0.116
FhI	5	12.6	7.01	35.1	2.79
	7	8.56	1.65	8.23	0.961
FG4$_d$hI	5	11.6	22.9	115	9.91
	7	7.78	9.42	47.1	6.05

To go a step further, several other factors were investigated: *i*- the temperature: FG4$_d$hI displays an excellent resistance as its activity is 45% maintained at 95°C for 120 min, without any change in particle size (*ca*. 330 nm at both room temperature and 95°C) (**Figure S12**); *ii*- the recyclability: FG4$_d$hI is efficiently recycled, as it retains >75% of its catalytic activity after 6 recycling (centrifugation) cycles (**Figure S13**); *iii*- the long-term stability: the catalytic activity of AA-heminzyme remained above 70% after 30 days in aqueous solution (**Figure S14**); *iv*- the substrate tolerance: FG4$_d$hI oxidizes 2 other substrates, 3,3′,5,5′-tetramethylbenzidine (TMB) and dopamine (DA), with an efficiency comparable to the oxidation of ABTS (**Figure S15**); *v*- the catalytic cost: the catalytic cost performance, here defined as the cost required for catalyzing 1 mole of substrate at maximum catalytic efficiency, was 5.8×10^6 to 2.5×10^5 €/$mol_{sub.}$ (depending on the manufacturer) for HRP, 9.3×10^6 €/$mol_{sub.}$ for CPDzyme,

and 2.4×10^7 €/mol_{sub} for G4/hemin. The catalytic cost was found to be dramatically decreased here, *i.e.*, 2.9×10^2 €/$mol_{sub.}$ for Fhl and 6.9×10^4 €/$mol_{sub.}$ for $FG4_dhI$, meaning that the costs of FhI and $FG4_dhI$ are 0.1 and 10% of that of HRP only, which makes it ideally suited to industrial applications (**Tables S7-S11**).

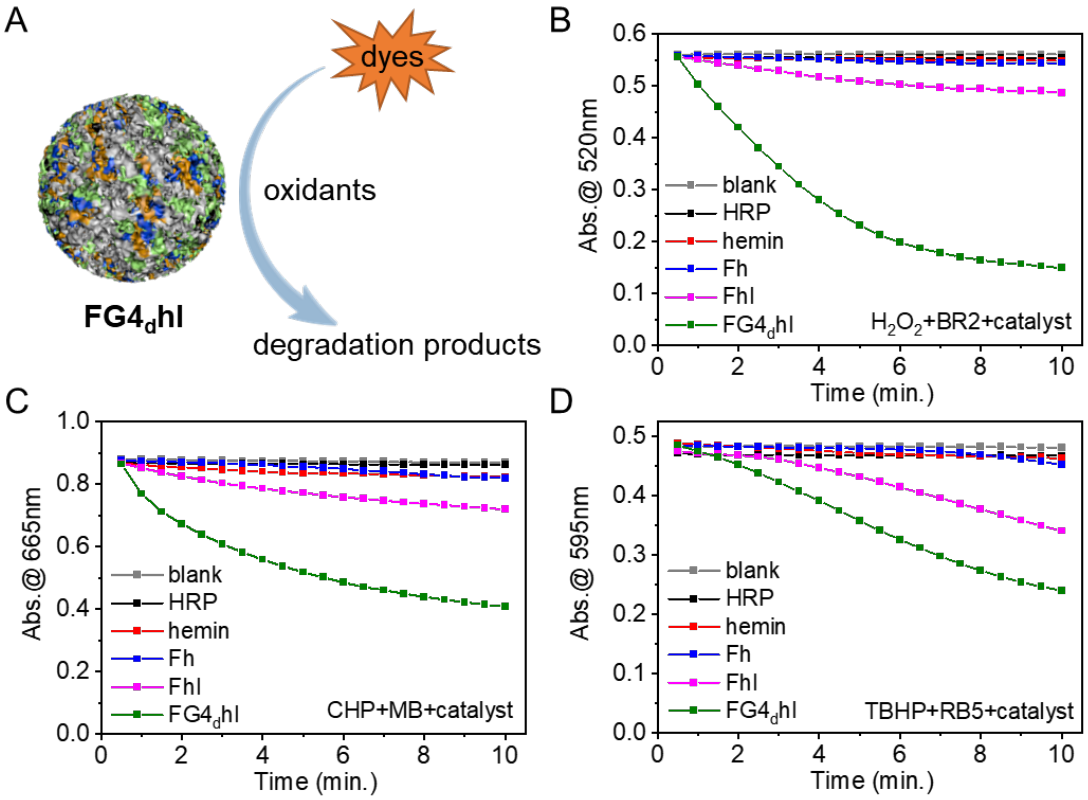

Figure 5. (A) Schematic representation of degradation of dye using various oxidants with $FG4_dhI$ as a catalyst. (B) Plot of maximum UV absorption versus time for BR2 decolorization by different catalysts with H_2O_2 as oxidant. (C) Plot of maximum UV absorption versus time for MB decolorization by different catalysts with CHP as oxidant. (D) Plot of maximum UV absorbance versus time for RB5 decolorization by different catalysts with TBHP as oxidant.

2.6. Applications of AA-heminzyme

To meet the requirements of practical industrial applications, the degradation of several dye used in the textile industry was studied,[22] including Basic Red 2 (BR2), N-containing dye Basic Blue 9 (BB9) and azo dye Reactive Black 5 (RB5). These dyes are commonly used for coloring paper, bamboo and wood products as well as for dyeing acrylic, cotton, linen and silk products, and are thus common pollutants found in printing and dyeing industry wastewaters.[23] Untreated wastewaters cannot be discharged into river systems as it can cause pollution and damage the ecosystem. Current physical, chemical and biological treatment strategies are effective, but with some drawbacks in terms of applicability, cost, efficacy, and time.[24] Three oxidants (hydrogen peroxide, cumyl hydroperoxide and tert-butyl hydroperoxide) and the three

dyes mentioned above were selected to assess the decolorization rates catalyzed by AA-heminzymes **(Figures S16)**. To this end, their UV absorbance was plotted against time (0 to 10 min) using different catalysts and oxidizers. As seen in **Figures 5** and **S17** (and **Table 2**), no significant changes were observed in the absence of catalyst ; interestingly, in these conditions, HRP had a decolorization rate of approximately 1%, that of hemin and Fh were also weak (<7%) while that of FhI reaches 12.6, 16.5 and 28.5% for BR2, BB9 and RB5, respectively, and that of $FG4_dhI$ was even higher (73.0, 51.5 and 50.7%, respectively). These results thus confirmed the actual application potential of AA-heminzymes.

Table 2. Dye decolorization rate (%) of three oxidants by different catalysts at pH 7 within 10 min.

	blank	HRP	hemin	Fh	FhI	$FG4_dhI$
H_2O_2-BR2	0.359	1.11	1.25	2.59	12.6	73.0
CHP-BB9	0.583	1.02	4.86	5.94	16.5	51.5
TBHP-RB5	0.525	0.895	5.15	6.37	28.5	50.7

To go a step further, a luminescent substrate, luminol (L), was incorporated in $FG4_dhI$, to obtain the chemiluminescent material $FG4_dhIL$ (**Figure 1**B). We aimed at using this assembly to visually detect disease-related biomarkers: as seen in **Figures S18** and **S19**, $FG4_dhIL$ exhibited stronger chemiluminescence (CL) intensity than the corresponding mixture of $FG4_dhI$+L over a wide range of pH (from 4 to 11). As an example, the CL intensity of $FG4_dhI$+L was only 8.4% of that of $FG4_dhIL$ at pH 6, **Figure S19**), while it is found much higher when pH ≥10, likely because the luminol, whose oxidation is known to be optimized under alkaline conditions, is less accessible when embedded in the nanoparticles. We also investigated the optimal hemin: L ratio, found to be 1:6 at pH 7 (**Figure S20**). Under these optimized conditions, we implemented the $FG4_dhIL$ system to detect glutathione (GSH), a well-established biomarker of cancer[25] and Alzheimer's disease.[26] The efficiency of this approach relies on the H_2O_2-mediated oxidation of GSH, which triggers a strong decrease of CL intensity. The optimal detection conditions for GSH were pH = 7, 50 μM H_2O_2 and 25 nM $FG4_dhIL$ (**Figure S21**), and the limit of detection (LOD) was 0.194 nM (3σ/slope) (**Figure S22**A). This method has a lower LOD compared to previously reported fluorescence, electrochemical and colorimetric methods (**Table S12**). Therefore, the $FG4_dhIL$-H_2O_2 system could be used for the detection of GSH with good selectivity in real samples (**Figure S22**B).

Finally, to further exploit this unprecedented sensitivity, we assembled a point-of-care GSH detection test (POCT), using a smartphone device (**Figure 6**A): the image color was first

converted into RGB values using the ColorPicker application and the experimental points converted into a curve in order to determine a LOD, here found to be 3.33 µM (3 σ/slope) (**Figure 6**B). Importantly, this detection is not sensitive to the phone brand. We then used this new POCT for the detection of GSH in human serum and the results were compared with GSH Content Assay kit: as seen in **Figure 6**D and **Table S13**, the deviation rate was in the range of -8.19% ~6.67%, which is agreeable, for a cost decreased by *ca*. 98% (**Table S14**), which thus confirms the great application potential of AA-heminzymes.

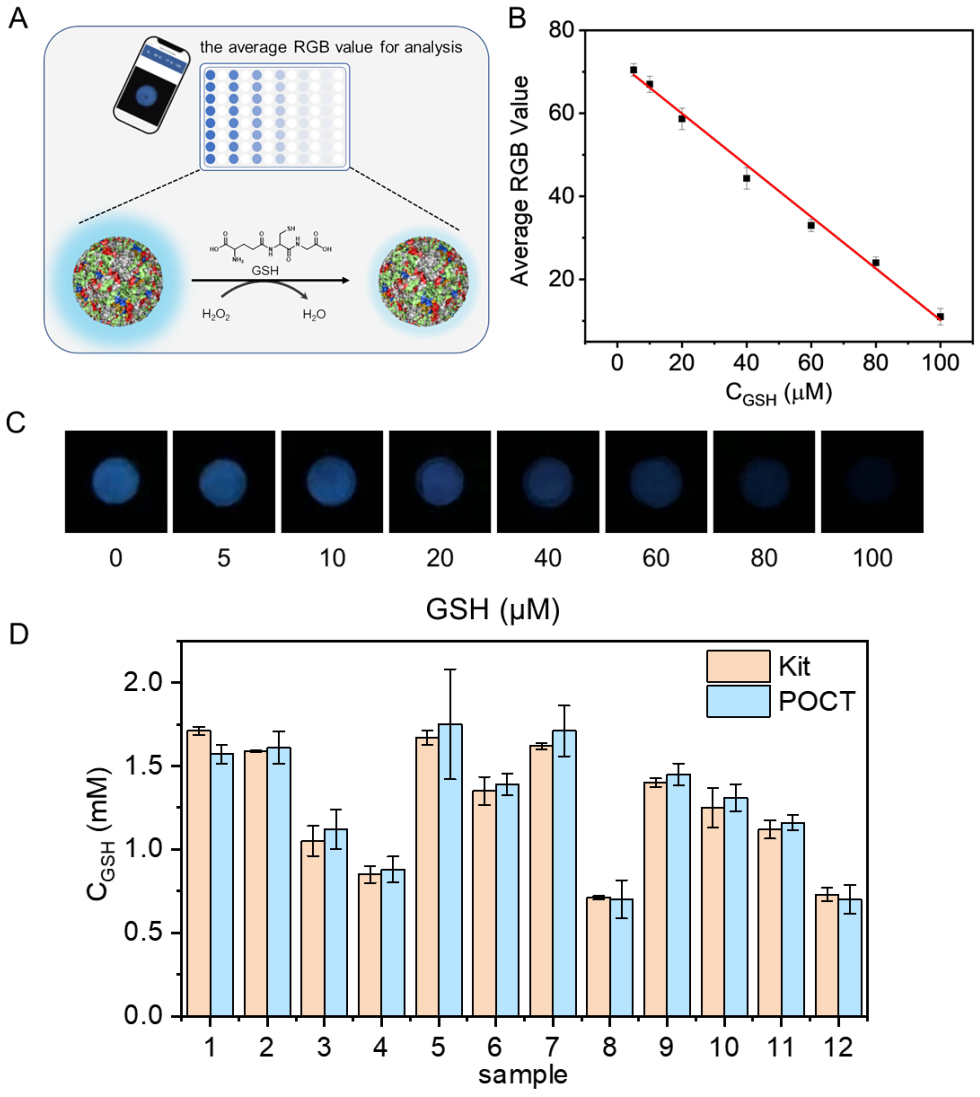

Figure 6. (A) Schematic representation of the smartphone-based detection of GSH by FG4$_d$hIL-H_2O_2. (B) Calibration curve of RGB value and GSH concentration, and the linear regression equation was y = -0.62 x + 73.33 (R^2 = 0.999). (C) Chemiluminescence photographs corresponding to different GSH concentrations. FG4$_d$hIL and GSH were added to 10 mM B-R buffer (pH 7.0). The distance between the cell phone and the sample was fixed, and 100 µL H_2O_2 was added to trigger the CL after ensuring the surrounding environment was dark. (D) Comparison of the POCT method and the kit for the detection of GSH concentration in human serum.

3. Conclusion

In conclusion, we designed and assembled a peroxidase-like mimetic enzyme referred to as AA-heminzyme in which His analogues and G4-forming sequences collaborate to provide hemin with an optimized environment suited to endow it with exquisite catalytic properties. The excellent performance of heminzyme was not only rationalized *in silico* but also demonstrated *in vitro*, the best prototype $FG4_dhI$ displaying a turnover number comparable to HRP. The ease of synthesis and the modularity of the assembly make heminzymes ideal candidates for future developments, which is further supported by both their highly catalytic efficiency and inexpensive nature. In addition, the system shows great versatility as different recognition elements (*e.g.*, aptamers or antibodies) can be conjugated wherever needed thanks to rather simple chemical modifications, either on the hemin core (using one of its two carboxylic arms) or on the G4 part for instance (conjugating the partner of interest on one of its two ends). The first two applications reported herein, *i.e.*, the catalytic degradation of industrial dyes (wastewater remediation) and the visual detection of glutathione biomarker (point-of-care testing), laid the first stones only in the construction of next-generation artificial enzymes, whose efficiency and versatility continue to be dazzlingly inventive.

Supporting Information

Supporting Information is available from the Wiley Online Library or from the author.

Acknowledgements

Dehui Qiu, Fangni He and Yuan Liu contributed equally to this work. This work was supported by the National Natural Science Foundation of China (22374070, 22177047, 21977045, 22004062, and 22104063), State Key Laboratory of Analytical Chemistry for Life Science (5431ZZXM2202), and the Fundamental Research Funds for the Central Universities (020514380299).

References

[1] a) N. A. Kotov, *Science* **2010**, *330*, 188–189; b) A. M. Alsharabasy, A. Pandit, P. Farras, *Adv. Mater.* **2021**, *33*, e2003883; c) X. Wang, Y. Hu, H. Wei, *Inorg. Chem. Front.* **2016**, *3*, 41-60.

[2] a) K. J. Koebke, T. B. J. Pinter, W. C. Pitts, V. L. Pecoraro, *Chem. Rev.* **2022**, *122*, 12046-12109; b) X. Zhang, D. Qiu, J. Chen, Y. Zhang, J. Wang, D. Chen, Y. Liu, M. Cheng, D. Monchaud, J. L. Mergny, H. Ju, J. Zhou, *J. Am. Chem. Soc.* **2023**, *145*, 4517-4526; c) M. Pott, T. Hayashi, T. Mori, P. R. E. Mittl, A. P. Green, D. Hilvert, *J. Am. Chem. Soc.* **2018**, *140*, 1535-1543.

[3] a) J. L. Mergny, D. Sen, *Chem. Rev.* **2019**, *119*, 6290-6325; b) M. L. Bochman, K. Paeschke, V. A. Zakian, *Nat. Rev. Genet.* **2012**, *13*, 770-780.

[4] a) P. Travascio, Y. Li, D. Sen, *Chem. Biol.* **1998**, *5*, 505-517; b) E. Golub, H. B. Albada, W. C. Liao, Y. Biniuri, I. Willner, *J. Am. Chem. Soc.* **2016**, *138*, 164-172; c) Y. Guo, J. Chen, M. Cheng, D. Monchaud, J. Zhou, H. Ju, *Angew. Chem. Int. Ed.* **2017**, *56*, 16636-16640.

[5] a) J. Xu, R. Jiang, H. He, C. Ma, Z. Tang, *Trends Anal. Chem.* **2021**, 139, 116257; b) H. Yang, Y. Zhou, J. Liu, *Trends. Anal. Chem.* **2020**,132, 116060.

[6] a) T. Jian, Y. Zhou, P. Wang, W. Yang, P. Mu, X. Zhang, X. Zhang, C. L. Chen, *Nat. Commun.* **2022**, *13*, 3025; b) Z.-G. Wang, H. Wang, Q. Liu, F. Duan, X. Shi, B. Ding, *ACS Catal.* **2018**, *8*, 7016-7024; c) Z. Ma, L. Yang, Y. Wang, M. Wang, W. Qi, Z. He, *Chem. Eng. J.* **2021**, *416*, 129149; d) W. Wu, Q. Wang, J. Chen, L. Huang, H. Zhang, K. Rong, S. Dong, *Nanoscale* **2019**, *11*, 12603-12609; e) T. Xue, B. Peng, M. Xue, X. Zhong, C. Y. Chiu, S. Yang, Y. Qu, L. Ruan, S. Jiang, S. Dubin, R. B. Kaner, J. I. Zink, M. E. Meyerhoff, X. Duan, Y. Huang, *Nat. Commun.* **2014**, *5*, 3200; f) Q. Xin, X. Jia, A. Nawaz, W. Xie, L. Li, J. R. Gong, *Nano Res.* **2020**, *13*, 1427-1433; g) Q. Wang, Z. Yang, X. Zhang, X. Xiao, C. K. Chang, B. Xu, *Angew. Chem. Int. Ed.* **2007**, *46*, 4285-4289; h) K. J. Koebke, T. Kuhl, E. Lojou, B. Demeler, B. Schoepp-Cothenet, O. Iranzo, V. L. Pecoraro, A. Ivancich, *Angew. Chem. Int. Ed.* **2021**, *60*, 3974-3978; i) J. Guo, Y. Liu, J. Zha, H. Han, Y. Chen, Z. Jia, *Polym. Chem.* **2021**, *12*, 858-866.

[7] Q. Liu, K. Wan, Y. Shang, Z. Wang, Y. Zhang, L. Dai, C. Wang, H. Wang, X. Shi, D. Liu, B. Ding, *Nat. Mater.* **2021**, *20*, 395–402.

[8] a) F. Krainer, A. Glieder. *Appl. Microbiol. Biotechnol.* **2015**, *99*, 1611–1625. b) D. Humer, J. Ebner, O. Spadiut. *Int. J. Mol. Sci.* **2020**, *21*, 4625.

[9] Y. Luo, M. Pehrsson, L. Langholm, M. Karsdal, A. Bay-Jensen, S. Sun. *Diagnostics* **2023**, *13*, 1835.

[10] a) T. L. Poulos, *Chem. Rev.* **2014**, *114*, 3919-3962; b) N. C. Veitch, *Phytochemistry* **2004**, *65*, 249-259; c) J. H. Dawson, *Science* **1988**, *240*, 433-439; d) J. S. de Ropp, S. Sham, A. Asokan, S. L. Newmyer, P. R. Ortiz de Montellano, G. N. La Mar, *J. Am. Chem. Soc.* **2002**, *124*, 11029-11037.

[11] C. Yuan, W. Ji, R. Xing, J. Li, E. Gazit, X. Yan, *Nat. Rev. Chem.* **2019**, *3*, 567-588.

[12] J. Smalley, A. Birss, R. Withnall, J. Silver, *Biochem. J.* **2002**, *362*, 239-245.

[13] a) K. Liu, R. Xing, Y. Li, Q. Zou, H. Mohwald, X. Yan, *Angew. Chem. Int. Ed.* **2016**, *55*, 12503-12507; b) K. Liu, C. Yuan, Q. Zou, Z. Xie, X. Yan, *Angew. Chem. Int. Ed.* **2017**, *56*, 7876-7880.

[14] a) S. Ozaki, I. Hara, T. Matsui, Y. Watanabe, *Biochemistry* **2001**, *40*, 1044-1052; b) P. K. Shantha, G. S. S. Saini, H. H. Thanga, A. L. Verma, *J. Raman Spectrosc.* **2001**, *32*, 159-165.

[15] a) A. Chatterjee, C. Mahato, D. Das, *Angew. Chem. Int. Ed.* **2021**, *60*, 202-207; b) R. Geng, R. Chang, Q. Zou, G. Shen, T. Jiao, X. Yan, *Small* **2021**, *17*, 2008114; c) S. Liu, S. Qiao, T. Yan,

X. Li, S. Yu, H. Sun, J. Xu, J. Liu, *Chem. Eng. J.* **2022**, *429*, 132592; d) H. Ahmadzade Kermani, A. Shockravi, Z. Moosavi-Movahedi, A. Khalafi-Nezhad, S. Behrouz, F.-Y. Tsai, G. H. Hakimelahi, A. Seyedarabi, A. A. Moosavi-Movahedi, *J. Iran Chem. Soc.* **2013**, *10*, 961-968; e) P. M. Punt, G. H. Clever, *Chem. Sci.* **2019**, *10*, 2513-2518; f) A. Rodriguez-Abetxuko, P. Muñumer, M. Okuda, J. Calvo, M. Knez, A. Beloqui, *Adv. Funct. Mater.* **2020**, *30*, 2002990; g) Z. Xu, L. Zhang, M. Pan, Q. Jiang, Y. Huang, F. Wang, X. Liu, *Adv. Funct. Mater.* **2021**, *31,* 2104100; h) L. Zhang, C. Gu, J. Xiong, M. Yang, Y. Guo, *Sci. China Chem.* **2014**, *58*, 731-737; i) J. Ji, Y. Chung, K. Hyun, K. Y. Chung, Y. Kwon, *J. Ind. Eng. Chem.* **2020**, *88*, 366-372.

[16] a) J. Eberhardt, D. Santos-Martins, A. F. Tillack, S. Forli, *J. Chem. Inf. Model.* **2021**, *61*, 3891-3898; b) O. Trott, A. J. Olson, *J. Comput. Chem.* **2010**, *31*, 455-461.

[17] a) S. Emamian, T. Lu, H. Kruse, H. Emamian, *J. Comput. Chem.* **2019**, *40*, 2868-2881; b) T. Lu, F. Chen, *J. Comput. Chem.* **2012**, *33*, 580-592.

[18] a) X. Mao, D. Qiu, S. Wei, X. Zhang, J. Lei, J. L. Mergny, H. Ju, J. Zhou, *ACS Appl. Mater. Interfaces* **2022**, *14*, 54598-54606; b) S. Nakayama, J. Wang, H. O. Sintim, *Chem. Eur. J.* **2011**, *17*, 5691-5698.

[19] a) D. Qiu, J. Mo, Y. Liu, J. Zhang, Y. Cheng, X. Zhang, *Molecules* **2020**, *25,* 3425; b) J. Chen, Y. Zhang, M. Cheng, Y. Guo, J. Šponer, D. Monchaud, J. L. Mergny, H. Ju, J. Zhou, *ACS Catal.* **2018**, *8*, 11352-11361.

[20] J. Chen, J. Wang, S. C. C. van der Lubbe, M. Cheng, D. Qiu, D. Monchaud, J. L. Mergny, C. F. Guerra, H. Ju, J. Zhou, *CCS Chem.* **2021**, *3*, 2183-2193.

[21] a) J.N. Rodriguez-Lopez, M.A. Gilabert, J. Tudela, R.N.F. Thorneley, F. GarciaCanovas, *Biochemistry* **2000**, *39*, 13201-13209; b) L. Fruk, J. Muller, C. M. Niemeyer, *Chem. Eur. J.* **2006**, *12*, 7448-7457; c) J. K. Kamal, D. V. Behere, *J. Inorg. Biochem.* **2003**, *94*, 236-242.

[22] a) S. Akhtar, A. A. Khan, Q. Husain, *Chemosphere* **2005**, *60*, 291-301; b) J. Z. Liu, T. L. Wang, L. N. Ji, *J. Mol. Catal. B Enzym.* **2006**, *41*, 81-86; c) S. M. Ulson de Souza, E. Forgiarini, A. A. Ulson de Souza, *J. Hazard. Mater.* **2007**, *147*, 1073-1078.

[23] a) S. Payra, S. Challagulla, Y. Bobde, C. Chakraborty, B. Ghosh, S. Roy, *J. Hazard. Mater.* **2019**, *373*, 377-388; b) X. Zhang, H. Song, Y. Chen, M. Zhuang, W. Liu, *Int. Biodeterior. Biodegrad.* **2021**, *157,* 105142.

[24] a) Crini, G. *Bioresour. Technol.* **2006**, *97*, 1061-1085; b) Zhang, L.; Leung, M.; Boriskina, S.; Tao, X. *Nat. Sustain.* **2023**, *6*, 243-253.

[25] N. Traverso, R. Ricciarelli, M. Nitti, B. Marengo, A. L. Furfaro, M. A. Pronzato, U. M. Marinari, C. Domenicotti, *Oxid. Med. Cell. Longev.* **2013**, *2013*, 972913.

[26] C. H. Lin, H. Y. Lane, *Antioxidants* **2021**, *10,* 1839.